Impact of a Jahn-Teller-like correlation coupling on the properties of mixed-valent SmB_6

O. Brandt
Institut für Theoretische Physik der Universität Stuttgart, Pfaffenwaldring 57, D-70550 Stuttgart, Germany

E. Sigmund
Institut für Theoretische Physik der Universität Stuttgart, Pfaffenwaldring 57, D-70550 Stuttgart, Germany and Institut für Physik, Technische Universität Cottbus, Karl Marx Straße 17, D-03046 Cottbus, Germany

M. Wagner
Institut für Theoretische Physik der Universität Stuttgart, Pfaffenwaldring 57, D-70550 Stuttgart, Germany
(Received 11 March 1998)

In previous studies a new type of Jahn-Teller coupling in doped SmB_6 was presented both in a molecular and in an extended semiconductor model. The conventional role of configurational distortions is taken over by a symmetry-adapted electronic-correlation coupling, which takes advantage of the electronic properties of the host crystal. Within this model electron spin-resonance measurements of the systems SmB_6:Gd^{3+} and SmB_6:Er^{3+} can be explained in a natural way. In this paper we examine the impact of this coupling-type on the properties of the band states. This results in a strong ''softening'' of the band states at the edge of the semiconducting gap and a contribution to the specific heat, which could serve as an additional experimental proof for the unconventional mechanism. [S0163-1829(98)04340-9]

I. INTRODUCTION

In preceding papers,[1,2] a species of a Jahn-Teller phenomenon was considered, in which spatially degenerate defect states are coupled to symmetry-adapted electronic excitations in a mixed-valent host crystal. The experimental motivation for this model is based on electron spin-resonance (ESR) measurements in the systems: SmB_6:$Er^{3\dagger}$ (Ref. 3) and SmB_6:$Gd^{3\dagger}$,[4] where unexpected spectra were measured at temperatures below 5–6 K. In the case of the $Gd^{3\dagger}$ defect a multiline spectrum could approximately be explained by the hypothesis of an electron capture in a Gd $5d$ orbital. As a result, the low-temperature spectrum was interpreted by a Gd^{2+} ground-state configuration. The spectrum in the Er defect case can be explained by a Γ_8 crystal-field ground state, which in the mixed-valent host crystal SmB_6 lies energetically below a Γ_6 state. This is in contrast to the situation in isostructural compounds RB_6 (R=Ba, Ca, and Yb), where a Γ_6 state forms the ground state. Since the observed unexpected features were characteristic for the host crystal SmB_6 a coupling mechanism was suggested, which takes advantage of the remarkable electronic properties of this host crystal: valence-fluctuating transitions and a very small band gap of 3–4 meV.[5] Electronic transitions are in this surrounding, ''softer'' than corresponding excitations of optical phonons (21 meV),[6] and, therefore, adopt the role of the configurational distortion in the conventional Jahn-Teller effect.

Within a molecular model the energetic lowering of the Γ_8 ground state of the Er^{3+} defect and its unusual isotropic ESR spectrum could be explained by the correlation coupling mechanism.[1] The extension to a doped semiconductor model[2] revealed that the strongest energetic lowering is accomplished by a direct local coupling of the degenerate defect states to the localized Sm $4f$ states of the host crystal. This kind of coupling takes advantage of the magnitude of low-energetic Sm $4f$ excitations characterized by the huge partial density of $4f$ states at the band edges of the small band gap.[5] The case of the Gd defect was modeled by the inclusion of a transfer coupling between the defect states and surrounding Sm $5d$ states. Within this model the unconventional Jahn-Teller coupling offers the following mechanism for the electron capture in the E_g crystal-field state of the Gd $5d$ orbital. If the uncoupled E_g state lies within the conduction band near the band edge of the band gap, the correlation coupling leads to an energetic lowering of the defect level and beyond a critical coupling strength to an effective state within the band gap. Since Gd^{3+}, which substitutes a Sm ion, introduces an electron into the conduction band,[7] this localized defect level is occupied (electron capture). With increasing temperature the energetic lowering decreases and the level is shifted back into the range of the conduction band where the electron is delocalized. This behavior is in qualitative agreement with experimental results where the multiline ESR spectrum connected with the captured electron vanishes with increasing temperature.

In this paper we consider the impact mainly of the correlation coupling on the crystal properties. In the next section we present the doped semiconductor model. In Sec. III the Green's function of the band states is calculated, in Sec. IV we examine the change of the effective one-particle density of states, in Sec. V we examine the effect of the correlation coupling on the specific heat, and in Sec. VI the charge distribution is considered.

II. MODEL HAMILTONIAN

In the ideal host crystal SmB_6 the two Sm configurations $(4f)^6(5d)^0$ and $(4f)^5(5d)^1$ are energetically almost degenerate and virtual transitions between them take place. We model the electronic structure of this system as described in

Ref. 2 considering a strongly localized $4f$ state and a delocalized $5d$ state at each site of the octahedral Sm lattice. Within the slave-boson method in the mean-field approximation we receive a band structure of hybridized states with self-consistantly determined parameters. This leads to a lowering of the effective Sm $4f$ level energy, to a remarkable reduction of the hybridization constant, and consequently of the band gap. In this one particle picture the density of states shows strong maxima near the band gap of mainly $4f$ character.

To be complete we give here the formulas for the band structure of the ideal host crystal (for details see Ref. 2):

$$H_{\text{band}}=\sum_{\mathbf{k},l,\sigma}\tilde{\varepsilon}_{\mathbf{k}l}c^{\dagger}_{\mathbf{k}l\sigma}c_{\mathbf{k}l\sigma}+\Lambda_{\text{SB}}N(r^2+1), \tag{1}$$

$$\tilde{\varepsilon}_{\mathbf{k}1}=\tfrac{1}{2}(\tilde{\varepsilon}_f-\Lambda_{\text{SB}}+\tilde{\varepsilon}_{\mathbf{k}}-W_{\mathbf{k}}),$$

$$\tilde{\varepsilon}_{\mathbf{k}2}=\tfrac{1}{2}(\tilde{\varepsilon}_f-\Lambda_{\text{SB}}+\tilde{\varepsilon}_{\mathbf{k}}+W_{\mathbf{k}}), \tag{2}$$

$$W_{\mathbf{k}}=\{[\tilde{\varepsilon}_{\mathbf{k}}-(\tilde{\varepsilon}_f-\Lambda_{\text{SB}})]^2+4(rV)^2\}^{1/2}. \tag{3}$$

$\tilde{\varepsilon}_{\kappa}$ is the dispersion relation of the hybridized band states with operators $c^{\dagger}_{\kappa\sigma}$, $c_{\kappa\sigma}$ ($\kappa=\mathbf{k}1,\mathbf{k}2$; $\sigma=\pm\frac{1}{2}$), $\tilde{\varepsilon}_f$ is the potential energy of the pure Sm $4f$ states, and $\tilde{\varepsilon}_k$ is the dispersion relation of the pure Sm $5d$ states. Energy values are measured with respect to the chemical potential μ ($\tilde{\varepsilon}_i=\varepsilon_i-\mu$). Λ_{SB} and r, respectively, are the Lagrange multiplier and the thermal expectation value of bose operators derived from the slave-boson method, which together with the chemical potential are determined self-consistently.

The Gd and Er defects substitute a Sm ion and, therefore, obey octahedral symmetry. To keep the model simple we assume at the defect site two states with the same physical properties as the replaced Sm states and, additionally, a Jahn-Teller active E_g orbital. Because only spatial degrees of freedom are relevant in our coupling, we neglect the spin indices. In this way the E_g states can represent both the Gd $5d$ crystal-field state and the spatial part of the Er Γ_8 state.

The model Hamiltonian of the doped semiconductor model consists of the following three parts:

$$H=H_0+H_{t_d}+H_{\lambda}, \tag{4}$$

with

$$H_0=\sum_{\kappa}\tilde{\varepsilon}_{\kappa}c^{\dagger}_{\kappa}c_{\kappa}+\sum_{i=1,2}\tilde{\varepsilon}_0a^{\dagger}_ia_i, \tag{5}$$

$$H_{t_d}=t_d(C^{\dagger}_{1t_d}a_1+C^{\dagger}_{2t_d}a_2+\text{H.c.})$$

$$=t_d\sum_{\kappa}[\xi_{1t_d}(\kappa)c^{\dagger}_{\kappa}a_1+\xi_{2t_d}(\kappa)c^{\dagger}_{\kappa}a_2+\text{H.c.}], \tag{6}$$

$$H_{\lambda}=\lambda[(C^{\dagger}_0C_1+C^{\dagger}_1C_0)(a^{\dagger}_2a_2-a^{\dagger}_1a_1)$$
$$+(C^{\dagger}_0C_2+C^{\dagger}_2C_0)(a^{\dagger}_2a_1+a^{\dagger}_1a_2)]$$
$$=\lambda\sum_{\kappa,\kappa'}(c^{\dagger}_{\kappa}c_{\kappa'}+c^{\dagger}_{\kappa'}c_{\kappa})[\xi_0(\kappa)\xi_1(\kappa')(a^{\dagger}_2a_2-a^{\dagger}_1a_1)$$
$$+\xi_0(\kappa)\xi_2(\kappa')(a^{\dagger}_2a_1+a^{\dagger}_1a_2)]. \tag{7}$$

H_0 describes the uncoupled defect system. It consists of the H_{band} and the operators $a^{\dagger}_ia_i$ ($i=1,2$) of the E_g defect states with the potential energy $\tilde{\varepsilon}_0$.

H_{t_d} describes the transfer coupling between the E_g defect states and the E_g states of the surrounding ($C^{\dagger}_{it_d}$, C_{it_d}, $i=1,2$), which are established by the Sm $5d$ states. ξ_{it_d}, $i=1,2$ are the corresponding coefficients of the projection of the local states of the defect onto the surrounding band states. In the case of the Er defect the relevant orbital is derived from a strongly localized $(4f)^{11}$ configuration. Therefore, a strong Coulomb interaction U is effective. We consider the limit $U\rightarrow\infty$ by the introduction of a slave-boson field with operators $b^{\dagger}$, b, and the corresponding constraint

$$b^{\dagger}b+\sum_{i=1,2}a^{\dagger}_ia_i=1. \tag{8}$$

This restriction limits the Hilbert space of possible defect states to the unoccupied and the singly occupied states.[8,9] To be consistent with Eq. (8) the transfer coupling for the Er case has to be modified in the following way:

$$H'_{t_d}=t_d\sum_{\kappa}[\xi_{1t_d}(\kappa)c^{\dagger}_{\kappa}b^{\dagger}a_1$$
$$+\xi_{2t_d}(\kappa)c^{\dagger}_{\kappa}b^{\dagger}a_2+\text{H.c.}]. \tag{9}$$

Although the cases of the Gd and the Er defects differ with respect to the transfer coupling we will combine the calculations for both models in this paper and point out the emerging differences.

H_{λ} describes the unconventional Jahn-Teller coupling, where defect states are coupled to transitions between $4f$ states of the next Sm neighbors, which form linear combinations transforming a A_{1g} ($C^{\dagger}_0$,C_0) and E_g representation ($C^{\dagger}_i$,C_i, $i=1,2$). The analogy to the conventional $E\otimes\varepsilon$ Jahn-Teller problem is obvious, because the operators $C^{\dagger}_0C_1+\text{H.c.}$ and $C^{\dagger}_0+C_2+\text{H.c.}$ show the same transformation behavior as the Q_1 and Q_2 modes in the conventional coupling.

III. GREEN'S FUNCTION OF THE BAND STATES

To reveal the changes of the band-state properties induced by the transfer and the correlation coupling of the Er or Gd defects, respectively, we calculate the one-particle Zubarev Green's function of the band states by means of Mori's formalism. For this purpose we define the Mori scalar product in the following way:

$$[A(t)|A(t')]=\langle A(t)A^{\dagger}(t')+A^{\dagger}(t')A(t)\rangle_T. \tag{10}$$

The anticommutator Green's function in the Fourier space is linked to the corresponding Mori scalar product in the Laplace space by

$$\langle\langle A|A^{\dagger}\rangle\rangle_E=\frac{-i}{2\pi}\left(\frac{1}{z-i\mathcal{L}}A\middle|A\right)_{z=-iE}, \tag{11}$$

$$\mathcal{L}=[H,\cdot],$$
$$A=A(0),\quad E=\omega\pm i\epsilon,\quad \hbar=1. \tag{12}$$

The Mori scalar product in Eq. (11) obeys the evolution equation of Mori[10]

$$\left(\frac{1}{z-i\mathcal{L}}A\middle|A\right)=\frac{(A|A)}{z-i\omega_0+\tilde{M}(z)}, \tag{13}$$

where

$$\omega_0=(\mathcal{L}A|A)(A|A)^{-1}, \tag{14}$$

$$\tilde{M}(z)=\left(\frac{1}{z-Q\mathcal{L}Q}Q\mathcal{L}A\middle|Q\mathcal{L}A\right)(A|A)^{-1}, \tag{15}$$

$$Q=1-P, \tag{16}$$

$$PX=(X|A)(A|A)^{-1}A. \tag{17}$$

For the calculation of the Green's function of the band states we choose the observable $A=c_\kappa$. The static Mori scalar product, therefore, yields $(c_\kappa|c_\kappa)=1$. The Mori frequency ω_0 and the self-energy $\tilde{M}_\kappa(z)$ cannot be calculated exactly. We calculate the terms to second order in the coupling constants $w=t_d$, λ.

To determine ω_0 and $\tilde{M}_\kappa(E)$ we subdivide the Liouvillian $\mathcal{L}$ according to the three parts H_0, H_{t_d}, and H_λ in the Hamiltonian and find

$$\mathcal{L}^0 c_\kappa=-\tilde{\varepsilon}_\kappa c_\kappa, \tag{18}$$

$$\mathcal{L}^{t_d} c_\kappa=-t_d[\xi_{1t_d}(\kappa)a_1+\xi_{2t_d}(\kappa)a_2], \tag{19}$$

$$\mathcal{L}^{\lambda} c_\kappa=-\lambda\sum_{\kappa',\kappa''}(\delta_{\kappa,\kappa'}c_{\kappa''}+\delta_{\kappa,\kappa''}c_{\kappa'})\times[\xi_0(\kappa')\xi_1(\kappa'')(a_2^{\dagger}a_2-a_1^{\dagger}a_1)+\xi_0(\kappa')\xi(\kappa'')(a_2^{\dagger}a_1+a_1^{\dagger}a_2)]. \tag{20}$$

In the case of the Er defect we have, correspondingly,

$$\mathcal{L}'^{td} c_\kappa=-t_d[\xi_{1t_d}(\kappa)b^{\dagger}a_1+\xi_{2t_d}(\kappa)b^{\dagger}a_2]. \tag{21}$$

We receive ω_0 by forming the scalar products

$$(\mathcal{L}^0 c_\kappa|c_\kappa)=-\tilde{\varepsilon}_\kappa, \tag{22}$$

$$(\mathcal{L}^{t_d} c_\kappa|c_\kappa)=0, \tag{23}$$

$$(\mathcal{L}^{\lambda} c_\kappa|c_\kappa)=-\lambda[\xi_0(\kappa)\xi_1(\kappa)\langle a_2^{\dagger}a_2-a_1^{\dagger}a_1\rangle_T+\xi_0(\kappa)\xi_2(\kappa)\langle a_2^{\dagger}a_1+a_1^{\dagger}a_2\rangle_T]. \tag{24}$$

Since we consider only second-order terms for ω_0, this results in

$$\omega_0=-\tilde{\varepsilon}_\kappa+O(w^3). \tag{25}$$

In the calculation of the self-energy $\tilde{M}(z)$ the operators $Q\mathcal{L}c_\kappa$ are of first order in w. In the case of the transfer-coupling term we approximate the projected Liouvillian $Q\mathcal{L}Q$ in the resolvent by $\mathcal{L}$. In this way we can reduce the expression for the corresponding self-energy term $\tilde{M}_{\kappa t_d}(E)$ to the Green's function of the defect states

$$\tilde{M}_{\kappa t_d}(E)=t_d^2\xi_{Et_d}^2(\kappa)2\pi\langle\langle A_{\rm def}|A_{\rm def}^{\dagger}\rangle\rangle_E, \tag{26}$$

where $\tilde{M}(E)=-i\tilde{M}(z=-iE)$. The operator $A_{\rm def}$ is defined by $A_{\rm def}=a_i$ in the Gd case or by $A_{\rm def}=b^{\dagger}a_i$ in the Er case,[2] respectively.

In the calculation of the self-energy term derived from the correlation coupling, we consider only second-order terms in w and, therefore, replace $Q\mathcal{L}Q$ by $\mathcal{L}^0$. This results in

$$\tilde{M}_{\kappa\lambda}(E)=\lambda^2\langle O_{\rm def}\rangle_T\times\sum_{\kappa'}\frac{\xi_0^2(\kappa)\xi_E^2(\kappa')+\xi_0^2(\kappa')\xi_E^2(\kappa)}{E-\tilde{\varepsilon}_{\kappa'}}, \tag{27}$$

where $\langle O_{\rm def}\rangle_T$ is defined by

$$\langle O_{\rm def}\rangle_T=\langle a_1^{\dagger}a_1+a_2^{\dagger}a_2-2a_1^{\dagger}a_2^{\dagger}a_2a_1\rangle_T^0. \tag{28}$$

The Green's function of the band states now reads

$$\langle\langle c_\kappa|c_\kappa^{\dagger}\rangle\rangle_E=\frac{1}{2\pi}\frac{1}{E-\tilde{\varepsilon}_\kappa-[\tilde{M}_{\kappa t_d}(E)+\tilde{M}_{\kappa\lambda}(E)]}. \tag{29}$$

The calculation of $\langle O_{\rm def}\rangle$ leads to different results in the Gd and Er cases, because in the latter the defect occupation number is restricted. In Appendix A the thermal expectation values for the Er defect are determined in the limit of an infinitely strong Coulomb repulsion at the defect site. This leads to

$$\langle O_{\rm def}\rangle_T=\frac{2}{e^{\beta\tilde{\varepsilon}_0}+2}=\begin{cases}0 & \text{for } \tilde{\varepsilon}_0>0\\ 1 & \text{for } \tilde{\varepsilon}_0<0\end{cases}\quad \text{for } T=0 \text{ K}. \tag{30}$$

In the case of the Gd ion the defect occupation number is not restricted in our model. From symmetry requirements the correlation coupling is effective only for a singly occupied defect level, which transforms like a E_g representation. In this case the level is lowered in energy by $\delta\tilde{\varepsilon}_0$. The doubly occupied defect level, however, transforms like a A_2 representation without spatial degeneracy and, therefore, the Jahn-Teller-like correlation coupling is ineffective. We take into

account this behavior in the calculation of $\langle O_{\mathrm{def}}\rangle_T$ in the following way (see Appendix A):

$$\langle O_{\mathrm{def}}\rangle_T = \frac{2}{e^{\beta(\tilde{\varepsilon}_0-\delta\tilde{\varepsilon}_0)}+2+e^{-\beta\tilde{\varepsilon}_0}} = \begin{cases} 0 & \text{for } \tilde{\varepsilon}_0-\delta\tilde{\varepsilon}_0>0 \\ 1 & \text{for } \tilde{\varepsilon}_0-\delta\tilde{\varepsilon}_0<0, \quad \tilde{\varepsilon}_0>0 \text{ for } T=0 \text{ K.} \\ 0 & \text{for } \tilde{\varepsilon}_0<0 \end{cases} \tag{31}$$

Equations (30) and (31) show that the correlation coupling is effective at temperature $T=0$ K only for a singly occupied defect level. This is in agreement with the described symmetry considerations above, and with our results in the calculation of the Green's function of the defect states.

The changes in the Green's functions of the band states expressed by the self-energy terms are of order $O(1/N)$ (N is the number of lattice sites), because we consider only one defect ion in the system. To make the impact of the defect couplings to the band states more visible we consider the density of states in the next section.

IV. DENSITY OF STATES

The one-particle density of states is defined by the trace taken with the difference between the retarded and the advanced one particle Green's functions of the system. Formally, we can separate the trace according to the Hilbert space of the undisturbed defect and band states. In this section we consider the change in the density of band states, which is defined by

$$\Delta\varrho_{\mathrm{band}}(\omega) = \frac{i}{2\pi}\sum_{\kappa}\left\{\left[\frac{1}{E-\tilde{\varepsilon}_\kappa-\tilde{M}_\kappa(E)} - \frac{1}{E-\tilde{\varepsilon}_\kappa}\right]_{E=\omega+i\epsilon} - [\,\cdot\,]_{E=\omega-i\epsilon}\right\}. \tag{32}$$

Equation (32) is the starting point of our numerical calculations and the main results are shown in Fig. 1 for the Er and in Fig. 2 for the Gd defect case, respectively.

In our model we consider a band structure of the undisturbed system with a total bandwidth of $B\approx 6$ eV (ranged from ≈ -3 to ≈ 3 eV), and a band gap $E_{\mathrm{gap}}\approx 0.1$ eV centered around -0.7 eV. The parameters were chosen because of numerical reasons and give a qualitative picture of the band structure of the host crystal SmB_6. In Fig. 1 the change in the density of states in the energy range of the band gap for the Er defect case is shown for the defect parameter values $\lambda = 0.2$ eV and $t_d = 0.1$ eV. The figure shows huge maxima at the edge of the band gap, which are generated by the correlation coupling. They are energetically located in the range of the high Sm $4f$ partial density of states. We will show, below, analytically that in the thermodynamical limit these maxima diverge for $\epsilon\to 0_+$. Huge changes in the density of states as shown in Fig. 1 indicate that the band system becomes very soft under the influence of this coupling, leading to an instability at the edges of the band gap (Jahn-Teller instability).

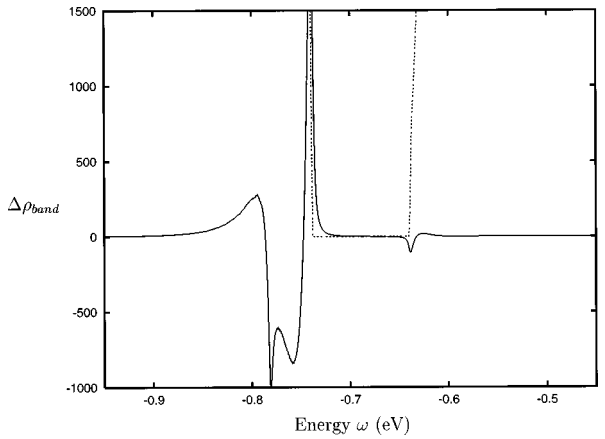

FIG. 1. Change of the effective one-particle density of states $\Delta\rho_{\mathrm{band}}(\omega)$ induced by the correlation coupling in the Er defect case. Band-continuum range $[\approx -3,\approx 3]$; dotted line, band gap. Defect parameters: $\varepsilon_0=\tilde{\varepsilon}_0+\mu=-1.8\lambda=0.2$, $t_d=0.1$, $\mu=-0.73$, $kT=0$.

In Fig. 2 the change in the density of band states for the Gd defect (full line) is compared with the corresponding change in the Er defect case (dotted line). Since the self-energy term $\tilde{M}_{\kappa\lambda}$ is independent of the potential energy of the defect level, the same shape of $\Delta\varrho_{\mathrm{band}}(\omega)$ appears in the band ranges close to the band edges in both cases. Within the band gap, however, a sharp peak shows up, which is located at the energy of the energetically lowered defect state. This contribution is caused by the transfer coupling and leads to admixtures of the band states to the effective defect state within the band gap.

To show the analytical behavior of $\Delta\varrho_{\mathrm{band}}(\omega)$ near the band edges we consider the case $t_d=0$ eV and transform Eq. (32) into

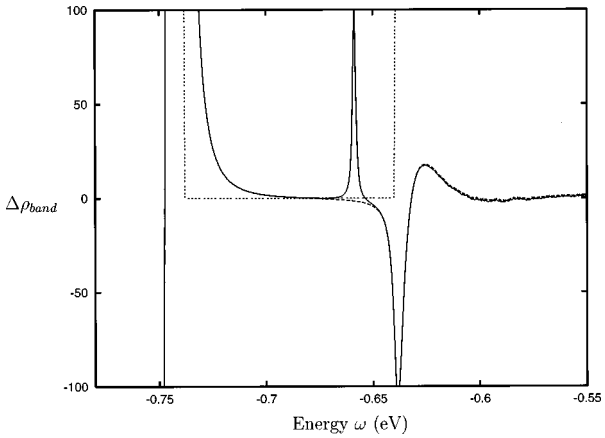

FIG. 2. Comparison of the change in the effective one-particle density of states $\Delta\rho_{\mathrm{band}}(\omega)$ induced by the correlation and by the transfer coupling for the Gd defect case (full line) and for the Er defect case (dotted line). Band-continuum range $[\approx -3,\approx 3]$; dotted line, band gap. Gd parameters: $\varepsilon_0=\tilde{\varepsilon}_0+\mu=-0.58\lambda=0.2$, $t_d=0.2$. Er parameters: $\varepsilon_0=\tilde{\varepsilon}_0+\mu=-1.8\lambda=0.2$, $t_d=0.2$, $\mu=-0.73$, $kT=0$.

$$\Delta\varrho_{\mathrm{band}}(\omega)=-\frac{1}{\pi}\,\mathrm{Im}\times\sum_{\kappa}\left.\frac{\tilde{M}_{\kappa\lambda}(E^{+})}{(E^{\dagger}-\tilde{\varepsilon}_{\kappa})[E^{\dagger}-\tilde{\varepsilon}_{\kappa}-\tilde{M}_{\kappa\lambda}(E^{\dagger})]}\right|_{E^{\dagger}=\omega+i\epsilon}. \tag{33}$$

Since the self-energy $\tilde{M}_{\kappa\lambda}(E)$ is of the order $O(1/N)$, the denominator can be developed into a series in the self-energy (ϵ finite). Because of the summation over κ the zeroth-order term remains finite while all other terms vanish in the thermodynamic limit ($N\to\infty$). When we convert the summation into an integration over the energy ω by the transformation $\Sigma_{\kappa}\to\int_{-\infty}^{\infty}\Sigma_{\kappa}\delta(\omega-\tilde{\varepsilon}_{\kappa})$, we receive

$$\Delta\varrho_{\mathrm{band}}(\omega)=-\frac{1}{\pi}\,\mathrm{Im}\int_{-\infty}^{\infty}d\omega'\,\frac{\tilde{M}_{\omega'}(E^{+})}{(E^{+}-\omega')^{2}}, \tag{34}$$

where $\tilde{M}_{\omega}$ is defined by

$$\tilde{M}_{\omega'}(E)=\lambda^{2}\langle O_{\mathrm{def}}\rangle_{T}\left\{\xi_{0}^{2}(\omega')\int_{-\infty}^{\infty}d\omega''\,\frac{\xi_{E}^{2}(\omega'')}{E-\omega''}+\xi_{E}^{2}(\omega')\int_{-\infty}^{\infty}d\omega''\,\frac{\xi_{0}^{2}(\omega'')}{E-\omega''}\right\}, \tag{35}$$

with

$$\xi_{0}^{2}(\omega)=\sum_{\kappa}\delta(\omega-\tilde{\varepsilon}_{\kappa})\xi_{0}^{2}(\kappa),\qquad \xi_{E}^{2}(\omega)=\sum_{\kappa}\delta(\omega-\tilde{\varepsilon}_{\kappa})[\xi_{1}^{2}(\kappa)+\xi_{2}^{2}(\kappa)]. \tag{36}$$

With the relation $(d/d\omega)[E-\omega]^{-1}=[E-\omega]^{-2}$ and by means of partial integration we receive

$$\Delta\varrho_{\lambda\mathrm{band}}(\omega)=\lambda^{2}\langle O_{\mathrm{def}}\rangle_{T}\left\{\left[\frac{d}{d\omega}\,\xi_{0}^{2}(\omega)\right]P\int_{-\infty}^{\infty}d\omega'\,\frac{\xi_{E}^{2}(\omega')}{\omega-\omega'}+\left[\frac{d}{d\omega}\,\xi_{E}^{2}(\omega)\right]P\int_{-\infty}^{\infty}d\omega'\,\frac{\xi_{0}^{2}(\omega')}{\omega-\omega'}+\xi_{0}^{2}(\omega)P\int_{-\infty}^{\infty}d\omega'\,\frac{\left[\frac{d}{d\omega'}\,\xi_{E}^{2}(\omega')\right]}{\omega-\omega'}+\xi_{E}^{2}(\omega)P\int_{-\infty}^{\infty}d\omega'\,\frac{\left[\frac{d}{d\omega'}\,\xi_{0}^{2}(\omega')\right]}{\omega-\omega'}\right\}. \tag{37}$$

In Eq. (37) the change in the density of states is dependent on the derivatives of the coupling coefficients $\xi_{i}^{2}(\omega)$. Near the band edges E_i of the gap the analytical behavior can be determined approximately and gives

$$\xi_{0}^{2}(\omega)\sim(|\omega-E_{i}|)^{1/2}, \tag{38}$$

$$\xi_{E}^{2}(\omega)\sim(|\omega-E_{i}|)^{5/2}. \tag{39}$$

Because $(d/d\omega)\xi_{0}^{2}\sim(|\omega-E_{i}|)^{-1/2}$ is valid the divergencies are exclusively due to the coefficient of the A_{1g} state of the defect surrounding. These are at the band edge, proportional to the density of states. The coefficients of the corresponding E_g states of the surrounding show a different analytical behavior and, therefore, exhibit no divergency.

V. SPECIFIC HEAT

In this section we determine the change in the internal energy ΔU and the resulting change of the specific heat ΔC_V induced by the Jahn-Teller-like correlation coupling ($\lambda\neq 0$; $t_d=0$). The internal energy U of the considered system is determined by the thermal expectation value of the Hamiltonian

$$U=\langle H\rangle_{T}=\sum_{\kappa}\tilde{\varepsilon}_{\kappa}\langle c_{\kappa}^{\dagger}c_{\kappa}\rangle_{T}+\sum_{i=1,2}\tilde{\varepsilon}_{0}\langle a_{i}^{\dagger}a_{i}\rangle_{T}+\lambda\sum_{\kappa\kappa'}\{\xi_{0}(\kappa)\xi_{1}(\kappa')\langle(c_{\kappa}^{\dagger}c_{\kappa'}+c_{\kappa'}^{\dagger}c_{\kappa})\times(a_{2}^{\dagger}a_{2}-a_{1}^{\dagger}a_{1})\rangle_{T}+\xi_{0}(\kappa)\xi_{2}(\kappa')\times\langle(c_{\kappa}^{\dagger}c_{\kappa'}+c_{\kappa'}^{\dagger}c_{\kappa})(a_{2}^{\dagger}a_{1}+a_{2}^{\dagger}a_{1})\rangle_{T}\}. \tag{40}$$

The expectation values $\langle c_{\kappa}^{\dagger}c_{\kappa}\rangle_{T}$ and in the Gd defect case of $\langle a_{i}^{\dagger}a_{i}\rangle$ can be determined by integration over the spectral function. This is defined in the following way for $\langle AB\rangle_{T}$:

$$\langle AB\rangle_{T}=\int_{-\infty}^{+\infty}d\omega\,\frac{\imath}{\exp(\beta\omega)+1}\times[\langle\langle B|A\rangle\rangle_{E}^{r}-\langle\langle B|A\rangle\rangle_{E}^{a}], \tag{41}$$

where β is the inverse temperature multiplied with the Boltzmann constant. In the Er defect case, where the restriction in Eq. (8) has to be obeyed, the expectation value of the defect occupation number can be determined using the defect Green's function $\langle\langle b^{\dagger}a_{i}|a_{i}^{\dagger}b\rangle\rangle_{E}$ defined in Eq. (26). This is possible because

$$\langle a_{i}^{\dagger}a_{i}\rangle_{T}=\langle a_{i}^{\dagger}a_{i}(bb^{\dagger}-b^{\dagger}b)\rangle_{T}=\langle b_{0'}a_{i}^{\dagger}a_{i}b_{0'}^{\dagger}\rangle_{T}. \tag{42}$$

In Eq. (42) the constraint [Eq. (8)] was used. To stay within the scope of this paper we consider the Er defect case at low temperatures where the assumption of a singly occupied defect level holds ($\langle a_{i}^{\dagger}a_{i}\rangle_{T}=\frac{1}{2}$, $\langle O_{\mathrm{def}}\rangle_{T}=1$).

To calculate the expectation value of the correlation coupling operator we exploit the equation of motion for $\langle\langle c_{\kappa}|c_{\kappa}^{\dagger}\rangle\rangle_{E}$:

$$(E-\tilde{\varepsilon}_\kappa)\langle\langle c_\kappa|c_\kappa^\dagger\rangle\rangle_E = \frac{1}{2\pi}+\sum_{\kappa'}\{[\xi_0(\kappa)\xi_1(\kappa')+\xi_0(\kappa')\xi_1(\kappa)] \times\langle\langle c'_\kappa(a_2^\dagger a_2-a_1^\dagger a_1)|c_\kappa^\dagger\rangle\rangle_E+[\xi_0(\kappa)\xi_2(\kappa') +\xi_0(\kappa')\xi_2(\kappa)]\langle\langle c'_\kappa(a_2^\dagger a_1-a_1^\dagger a_2)|c_\kappa\rangle\rangle_E\}. \tag{43}$$

Using Eq. (43) we can reduce the calculation of the internal energy of the interacting system to one particle Green's functions

$$U=\sum_{i=1,2}\tilde{\varepsilon}_0\langle a_i^\dagger a_i\rangle_T +\sum_\kappa\int_{-\infty}^{\infty}d\omega\,\frac{i}{e^{\beta\omega}+1} \times\omega[\langle\langle c_\kappa|c_\kappa^\dagger\rangle\rangle_{\omega+i\epsilon}-\langle\langle c_\kappa|c_\kappa^\dagger\rangle\rangle_{\omega-i\epsilon}]. \tag{44}$$

To compare this result with the outcome of the perturbation theory we introduce the one-pole approximation for the self-energy $\tilde{M}_\kappa(\omega=\tilde{\varepsilon}_\kappa)$. In this way we receive for the internal energy

$$U=\sum_{i=1,2}\tilde{\varepsilon}_0\langle a_i^\dagger a_i\rangle_T+\sum_\kappa[\tilde{\varepsilon}_\kappa+\mathrm{Re}\,\tilde{M}_{\kappa\lambda}(\tilde{\varepsilon}_\kappa)] \times f(\tilde{\varepsilon}_\kappa+\mathrm{Re}\,\tilde{M}_{\kappa\lambda}(\tilde{\varepsilon}_\kappa),T). \tag{45}$$

In the thermodynamic limit $f(\mathrm{Re}\,\tilde{M}_{\kappa\lambda}(\tilde{\varepsilon}_\kappa),T)=f(\tilde{\varepsilon}_\kappa,T)$ applies, where $f(\tilde{\varepsilon}_{\kappa'},T)=[\exp(\beta\tilde{\varepsilon}_{\kappa'})+1]^{-1}$. For a singly occupied defect level the correlation coupling results in the change of the internal energy with

$$\Delta U=-\lambda^2 P\sum_{\kappa\kappa'}\frac{\xi_0^2(\kappa)\xi_E^2(\kappa')+\xi_0^2(\kappa')\xi_E^2(\kappa)}{\tilde{\varepsilon}_{\kappa'}-\tilde{\varepsilon}_\kappa} \times f(\tilde{\varepsilon}_\kappa,T)[1-f(\tilde{\varepsilon}_{\kappa'},T)]. \tag{46}$$

For $T=0$ K the same result is received for a second-order perturbation calculation in the coupling constant λ. At very low temperatures only virtual transitions between conduction-band and valence-band states are possible in Eq. (46). Transitions between states close to the band gap with strong effective coupling coefficients $\xi_i^2(\kappa)$ lead to the strongest contributions to ΔU. Therefore, the direct coupling to the possible low-energetic $4f$ excitations in SmB_6 is advantageous for the correlation coupling mechanism.

The change of the internal energy results in a change of the specific heat defined by

$$\Delta C_V=\frac{\partial}{\partial T}\Delta U. \tag{47}$$

In Fig. 3 the change of the specific heat ΔC_V for the considered Er defect case is shown for different values of the coupling constant λ. The correlation coupling shifts the maximum of the specific heat to lower temperatures than the maximum of the ideal system at $kT\sim E_{\mathrm{gap}}$. Figure 3 shows

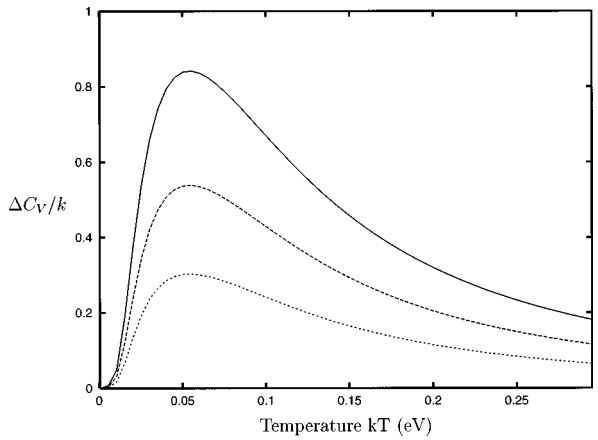

FIG. 3. Correlation-induced change in the specific heat $\Delta C_V(T)$ for the Er defect case for different values of the coupling constant. $\lambda=0.25$ (full line), $\lambda=0.2$ (broken line), and $\lambda=0.15$ (dotted line), $t_d=0{,}1$ (arbitrary units for both axes).

the effect of only one defect site. We can sum up these contributions for many sites in the limit of low-defect concentrations, where we can neglect the defect-defect interaction. In this way the correlation coupling-induced maximum in the specific heat should be measurable in dependence of the defect concentration. Thus, additionally to the ESR spectra, we have a measurable quantity for the evidence of the Jahn-Teller-like correlation-coupling mechanism.

VI. CHARGE DISTRIBUTION

Since the coefficients of the correlation coupling depend on crystal directions, we are interested in spatial effects of this mechanism. For this purpose we calculate the change in the charge density of the defect surroundings. This also enables us to determine the range of validity of the assumption of independent defect sites.

We consider the thermal expectation value $\Delta\overline{n_{\mathbf{i}}^{(d,f)}}$ defined by

$$\Delta\overline{n_{\mathbf{i}}^{(d)}}=\langle d_{\mathbf{i}}^\dagger d_{\mathbf{i}}\rangle_T^{H_0+W}-\langle d_{\mathbf{i}}^\dagger d_{\mathbf{i}}\rangle_T^{H_0}, \qquad \Delta\overline{n_{\mathbf{i}}^{(f)}}=\langle f_{\mathbf{i}}^\dagger f_{\mathbf{i}}\rangle_T^{H_0+W}-\langle f_{\mathbf{i}}^\dagger f_{\mathbf{i}}\rangle_T^{H_0}, \tag{48}$$

where $d_i^\dagger$, d_i and $f_i^\dagger$, f_i are the creation and annihilation operators of electrons in the Sm $5d$ and Sm $4f$ states at crystal site $\mathbf{i}$, respectively. The perturbation W consists only of the correlation coupling $(t_d=0)$. We can express Eq. (48) by the operators of the hybridized band states, yielding

$$\Delta\overline{n_{\mathbf{i}}^{(d,f)}}=\sum_{\kappa\kappa'}(\alpha_\kappa^{(d,f)})^* e^{-i\mathbf{k}\mathbf{i}}\alpha_{\kappa'}^{(d,f)}e^{i\mathbf{k}'\mathbf{i}} \times[\langle c_\kappa^\dagger c_{\kappa'}\rangle_T^{H_0+W}-\langle c_\kappa^\dagger c_{\kappa'}\rangle_T^{H_0}]. \tag{49}$$

The coefficients $\alpha_\kappa^{(d,f)}$ are given in Appendix B. The thermal expectation value $\langle c_\kappa^\dagger c_{\kappa'}\rangle_T^{H=H_0+W}$ is defined by

$$\langle c_\kappa^\dagger c_{\kappa'}\rangle_T^H=\frac{1}{Z}\,\mathrm{Tr}\{c_\kappa^\dagger c_{\kappa'}e^{-\beta H}\},\quad Z=\mathrm{Tr}\{e^{-\beta H}\}. \tag{50}$$

Applying a perturbation expansion in W to the thermal-density operator $(1/Z)\exp[-\beta(H_0+W)]$ we take into account terms in the second order in λ. This results in

$$\begin{aligned}\langle c_\kappa^\dagger c_{\kappa'}\rangle_T^{H_0+W}=&\langle c_\kappa^\dagger c_{\kappa'}\rangle_T^{H_0}\\&+\left\langle \int_0^\beta d\beta' W(\beta')[\langle c_\kappa^\dagger c_{\kappa'}\rangle_T^{H_0}-c_\kappa^\dagger c_{\kappa'}]\right\rangle_T^{H_0}\\&+\left\langle \int_0^\beta d\beta' W(\beta')\right\rangle_T^{H_0}\\&\times\left\langle \int_0^\beta \beta' W(\beta')[\langle c_\kappa^\dagger c_{\kappa'}\rangle_T^{H_0}-c_\kappa^\dagger c_{\kappa'}]\right\rangle_T^{H_0}\\&+\left\langle \int_0^\beta d\beta'\int_0^{\beta'} d\beta'' W(\beta')W(\beta'')\right.\\&\left.\times[c_\kappa^\dagger c_{\kappa'}-\langle c_\kappa^\dagger c_{\kappa'}\rangle_T^{H_0}]\right\rangle_T^{H_0}+O(W^3),\end{aligned}\tag{51}$$

$$W(\beta)=\lambda\sum_{\kappa\kappa'} e^{\beta(\tilde\varepsilon_\kappa-\tilde\varepsilon_{\kappa'})}c_\kappa^\dagger c_{\kappa'}\times[\tilde\xi(\kappa,\kappa')(a_2^\dagger a_2-a_1^\dagger a_1)+\tilde\xi(\kappa,\kappa')(a_2^\dagger a_1+a_1^\dagger a_2)],\tag{52}$$

$$\tilde\xi_i(\kappa,\kappa')=\xi_0(\kappa)\xi_i(\kappa')+\xi_0(\kappa')\xi_i(\kappa),\quad i=1,2.\tag{53}$$

Within this expansion expectation values that are of the first order in $W(\beta)$ are zero, because of the appearing thermal expectation values $\langle a_2^\dagger a_2-a_1^\dagger a_1^\dagger\rangle_T^{H_0}$ and $\langle a_2^\dagger a_1+a_1^\dagger a_2\rangle_T^{H_0}$. With the help of the theorem of Bloch and De Dominicis,[11] we can calculate the second-order term $\langle c_\kappa^\dagger c_{\kappa'}\rangle_T^{(2)}$ of the expansion. This yields

$$\begin{aligned}\langle c_\kappa^\dagger c_{\kappa'}\rangle_T^{(2)}=&\lambda^2\langle O_{\rm def}\rangle_T\sum_{\kappa''}\int_0^\beta d\beta'\\&\times\int_0^{\beta'} d\beta''[\tilde\xi_1(\kappa,\kappa'')\tilde\xi_1(\kappa'',\kappa')\\&+\tilde\xi_2(\kappa,\kappa'')\tilde\xi_2(\kappa'',\kappa')][e^{\beta'(\varepsilon_{\kappa'}-\varepsilon_{\kappa''})}e^{\beta''(\varepsilon_{\kappa''}-\varepsilon_\kappa)}\\&\times(1-\overline{f}_\kappa)(1-\overline{f}_{\kappa''})\overline{f}_{\kappa'}+e^{\beta'(\varepsilon_{\kappa''}-\varepsilon_\kappa)}e^{\beta''(\varepsilon_{\kappa'}-\varepsilon_{\kappa''})}\\&\times(1-\overline{f}_\kappa)\overline{f}_{\kappa''}\overline{f}_{\kappa'}],\end{aligned}\tag{54}$$

$$\overline{f}_\kappa=f(\tilde\varepsilon_\kappa,T).$$

Integrating over β' and β'' we receive

$$\begin{aligned}\langle c_\kappa^\dagger c_{\kappa'}\rangle_T^{(2)}=&\lambda^2\langle O_{\rm def}\rangle_T\sum_{\kappa''}[\tilde\xi_1(\kappa,\kappa'')\\&\times\tilde\xi_1(\kappa'',\kappa')+\tilde\xi_2(\kappa,\kappa'')\tilde\xi_2(\kappa'',\kappa')]\\&\times\left[\frac{e^{\beta\varepsilon_\kappa}(e^{\beta\varepsilon_{\kappa'}}-e^{\beta\varepsilon_{\kappa''}})-e^{\beta\varepsilon_{\kappa''}}+e^{\beta\varepsilon_\kappa}}{(\varepsilon_{\kappa''}-\varepsilon_\kappa)(\varepsilon_{\kappa''}-\varepsilon_{\kappa'})}\right.\\&+\frac{e^{\beta\varepsilon_{\kappa''}}(e^{\beta\varepsilon_{\kappa'}}-e^{\beta\varepsilon_\kappa})}{(\varepsilon_\kappa-\varepsilon_{\kappa'})(\varepsilon_\kappa-\varepsilon_{\kappa''})}+\left.\frac{e^{\beta\varepsilon_\kappa}-e^{\beta\varepsilon_{\kappa'}}}{(\varepsilon_{\kappa'}-\varepsilon_\kappa)(\varepsilon_{\kappa'}-\varepsilon_{\kappa''})}\right]\\&\times\overline{f}_\kappa\overline{f}_{\kappa''}\overline{f}_{\kappa'}.\end{aligned}\tag{55}$$

Expression (55) does not diverge for any $\tilde\varepsilon_\kappa=\tilde\varepsilon_{\kappa'}$ because of the corresponding contributions of the three summands. We can insert Eq. (55) into Eq. (51) and into Eq. (49) and receive for the change in the charge distribution, finally,

$$\begin{aligned}\Delta\overline{n}_{\mathbf{i}}^{(d,f)}=&\lambda^2\sum_{\kappa,\kappa',\kappa''}\langle O_{\rm def}\rangle_T(\alpha_\kappa^{(d,f)})^*\alpha_{\kappa'}^{(d,f)}\prod_{j=x,y,z}\cos(\mathbf{k}_j\mathbf{i}_j)\\&\times\cos(\mathbf{k}_j'\mathbf{i}_j)[\tilde\xi_1(\kappa,\kappa'')\tilde\xi_1(\kappa'',\kappa')\\&+\tilde\xi_2(\kappa,\kappa'')\tilde\xi_2(\kappa'',\kappa')]\\&\times\left[\frac{\overline{f}_\kappa(1-\overline{f}_{\kappa''})(1-\overline{f}_{\kappa'})}{(\varepsilon_\kappa-\varepsilon_{\kappa'})(\varepsilon_\kappa-\varepsilon_{\kappa''})}+\frac{(1-\overline{f}_\kappa)(1-\overline{f}_{\kappa''})\overline{f}_{\kappa'}}{(\varepsilon_{\kappa'}-\varepsilon_\kappa)(\varepsilon_{\kappa'}-\varepsilon_{\kappa''})}\right.\\&\left.+\frac{(1-\overline{f}_\kappa)\overline{f}_{\kappa''}(1-\overline{f}_{\kappa'})}{(\varepsilon_{\kappa''}-\varepsilon_\kappa)(\varepsilon_{\kappa''}-\varepsilon_{\kappa'})}\right].\end{aligned}\tag{56}$$

In Eq. (56) the evenness of the κ-dependent functions was utilized. The symmetry of the coefficients $\xi_i^2(\kappa)$ $(i=0,1,2)$ leads under the summation over κ'' to the following simplification:

$$\begin{aligned}&\sum_{\kappa''}[\tilde\xi_1(\kappa,\kappa'')\tilde\xi_1(\kappa'',\kappa')+\tilde\xi_2(\kappa,\kappa'')\tilde\xi_2(\kappa'',\kappa')]f(\kappa,\kappa'',\kappa')\\&=\sum_{\kappa''}\{\xi_0^2(\kappa'')[\xi_1(\kappa)\xi_1(\kappa')+\xi_2(\kappa)\xi_2(\kappa')]\\&\quad+\xi_0(\kappa')\xi_E^2(\kappa'')\xi_0(\kappa')\}f(\kappa,\kappa'',\kappa').\end{aligned}\tag{57}$$

Equation (57) shows that $\Delta\overline{n}_i^{d,f}$ is invariant under the symmetry operations of the octahedral group. For the temperature $T=0$ K the change in the charge density is only due to virtual transitions between the valence-band and conduction-band states. The low-energetic Sm $4f$ excitations are, as in the lowering of the internal energy, the most important contributions.

It is noteworthy that Eq. (56) can also be derived by the calculation of the corresponding Green's functions with the help of a matrix version of the formalism of Mori's formalism. Equation (56) in this case is reestablished in the thermodynamic limit.

In Fig. 4 the change in the charge density in the defect surrounding is shown for $\Delta\overline{n}_{\mathbf{i}}^{(f)}$ [Fig. 4(a)] and $\Delta\overline{n}_{\mathbf{i}}^{(d)}$ [Fig. 4(b)], respectively. The full and shadowed circles indicate the positive and negative sign, respectively, while the area is proportional to the absolute value of $\Delta\overline{n}_{\mathbf{i}}^{(f,d)}$. The first octant

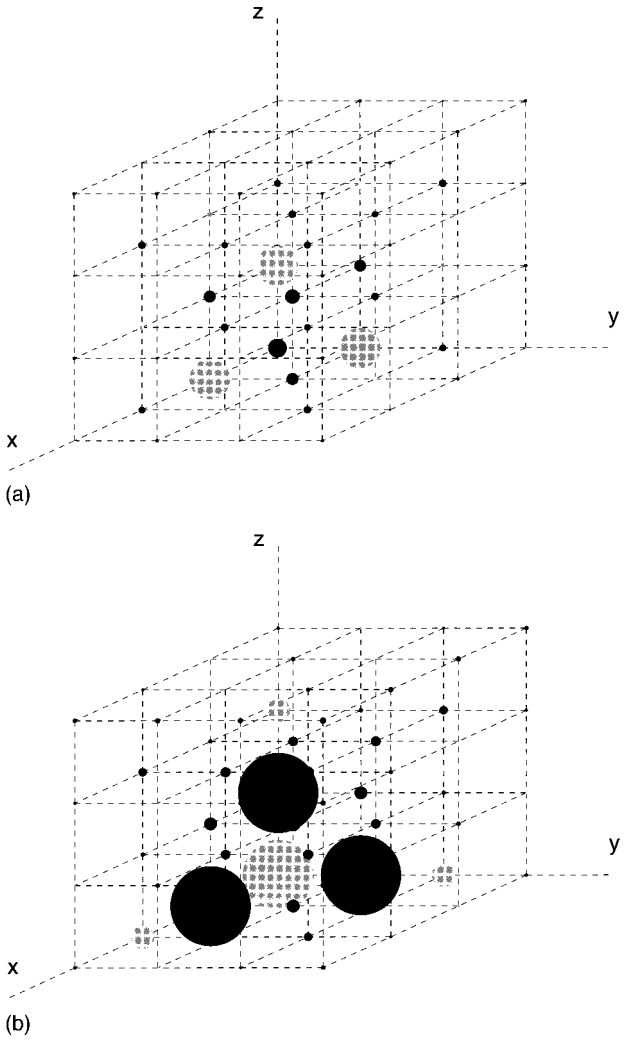

FIG. 4. Change of the partial Sm charge density $\Delta\overline{n}_{\mathbf{i}}^{(f,d)}$ of the defect surrounding induced by the correlation coupling in the Er defect case. Shown is the first octant with the defect at the origin. Full (positive) and shadowed (negative) circles show the sign, the circle area indicates the absolute value. (a) Partial Sm $4f$ charge density, maximum value at site $\mathbf{i}=(1,0,0)$, $\Delta\overline{n}_{100}^{(f)}/\lambda^2=0.28$. (b) Partial Sm $5d$ charge density, maximum value at site $\mathbf{i}=(1,0,0)$, $\Delta\overline{n}_{100}^{(d)}/\lambda^2=-0.07$.

of the defect surrounding is shown with the defect site at the origin. The strongest increase of $4f$ charge density [Fig. 4(a)] appears at the nearest-neighbor sites. With the corresponding local states the correlation coupling was built up in the local picture. Because these states are part of the hybridized band states the charge density is changed also at other sites and, additionally, in the partial $5d$ charge density. With increasing site distance the effect of the correlation coupling falls off very rapidly, with the exception of the crystal axes where a small oscillation of the charge density appears. At the defect site, where we have assumed two states with the same properties as the surrounding Sm states, additionally to the Jahn-Teller active E_g states, the $4f$ charge density is decreased. The effect of the correlation coupling on the $4f$ charge density is partially compensated by the change of the $5d$ contributions as shown in Fig. 4(b). It should be stressed that, although $\Delta\overline{n}_{\mathbf{i}}^{(d,f)}$ is invariant under symmetry transformations of the O_h group, it is not radially isotropic, but dependent on the crystal directions. If we assume that the defect sites build a regular lattice, the defect-defect interaction can be neglected up to a distance of ≈ 5 lattice constants.

VII. CONCLUSION

In this paper we have examined the impact of a correlation coupling and of a transfer coupling on the band states of a doped mixed-valent semiconductor. The correlation mechanism establishes a Jahn-Teller-like coupling, where electronic excitations adopt the role of the configurational distortion in the conventional case. The calculation of the internal energy showed that for temperature $T=0$ K virtual transitions between valence-band and conduction-band states lead to a lowering of the energy. Since the host crystal SmB_6 has a very small band gap of $E_{\mathrm{gap}}\approx 3$–$4$ meV and a very huge partial density of Sm $4f$ states at the corresponding band edges, this electronic coupling-type is very effective when the low-energetic $4f$ excitations are involved. This is in agreement with the result of the calculation of the defect Green's function. In the host crystal SmB_6 the electronic coupling is, therefore, more probable than the conventional type of configurational coupling.

For higher temperatures, conduction-band states become populated and, therefore, the effective number of possible low-energetic excitations decrease. This leads to a decrease of the coupling-induced energetic lowering of the internal energy and, consequently, to a typical change of the specific heat. This change of the specific heat has a maximum value for $kT\approx 0.5E_{\mathrm{gap}}$. This peak could be measurable in dependence of the defect concentration and provides an additional means to proof the unconventional coupling mechanism.

The effect of the correlation coupling on the charge distribution falls off rapidly with increasing distance between the defect and the Sm ions. There are strong changes of the partial $4f$ charge density, which are to some extent compensated by the changes of the partial $5d$ charge density at the same crystal site.

ACKNOWLEDGMENT

The authors would like to thank the Deutsche Forschungsgemeinschaft for financial support.

APPENDIX A: CALCULATION OF $\langle O_{\mathrm{def}}\rangle$

We calculate the expectation values $\langle a_i^\dagger a_i\rangle_T$ and $\langle a_1^\dagger a_2^\dagger a_1 a_2\rangle_T$ with the Hamiltonian

$$H=H_0+H_U \quad \text{with} \quad H_U=Ua_1^\dagger a_2^\dagger a_2 a_1. \tag{A1}$$

H_0 is defined in Eq. (5). Our procedure is analogous to the proof of the theorem of Bloch and De Dominicis. For this purpose we need

$$e^{\beta(H_0+H_U)}a_i^\dagger e^{-\beta(H_0+H_U)} = e^{\beta\tilde{\varepsilon}_0}[a_i^\dagger+(\delta_{i,1}a_1^\dagger a_2^\dagger a_2+\delta_{i,2}a_2^\dagger a_2^\dagger a_1)(e^{\beta U}-1)]. \tag{A2}$$

With the help of the anticommutator relation for the Fermi operators and with Eq. (A2), we receive the following relation between the considered expectation values:

$$\langle a_i^\dagger a_i\rangle_T=\frac{1}{1+e^{\beta\tilde{\varepsilon}_0}}-\frac{(e^{\beta U}-1)e^{\beta\tilde{\varepsilon}_0}}{e^{\beta\tilde{\varepsilon}_0}+1}\langle a_1^\dagger a_2^\dagger a_1 a_2\rangle_T. \tag{A3}$$

For Eq. (A3) the property of cyclic interchangeability of operators under the trace was used.

Applying analogous steps to the expectation value $\langle a_1^\dagger a_2^\dagger a_2 a_1\rangle_T$ yields a second relation between the requested expectation values

$$\langle a_1^\dagger a_2^\dagger a_2 a_1\rangle_T=\frac{1}{1+e^{\beta\tilde{\varepsilon}_0}e^{\beta U}}\langle a_1^\dagger a_1\rangle_T. \tag{A4}$$

With Eqs. (A3) and (A4) we finally receive

$$\langle a_1^\dagger a_1\rangle_T=\langle a_2^\dagger a_2\rangle_T=\frac{e^{\beta(\tilde{\varepsilon}_0+U)}+1}{e^{\beta(2\tilde{\varepsilon}_0+U)}+2e^{\beta(\tilde{\varepsilon}_0+U)}+1}, \tag{A5}$$

$$\langle a_1^\dagger a_2^\dagger a_2 a_1\rangle_T=\frac{1}{e^{\beta(2\tilde{\varepsilon}_0+U)}+2e^{\beta(\tilde{\varepsilon}_0+U)}+1}. \tag{A6}$$

In the case of the Er defect we have to take the limit $U\to\infty$ in agreement with the applied slave-boson method. This yields

$$\langle a_i^\dagger a_i\rangle_T=\frac{1}{e^{\beta\tilde{\varepsilon}_0}+2}, \tag{A7}$$

$$\langle a_1^\dagger a_2^\dagger a_2 a_1\rangle_T=0. \tag{A8}$$

In the case of the Gd defect we take the energetic lowering of the singly occupied defect level into account. We fix the value of the energetic lowering $\delta\tilde{\varepsilon}_0$ with the self-energy of the defect Green's function $\delta\tilde{\varepsilon}_0=\tilde{M}_{\rm def}(\tilde{\varepsilon}_0)<0$.[2] In this case we have to replace the parameters in the preceeding calculation with $\tilde{\varepsilon}_0\to\tilde{\varepsilon}_0+\tilde{M}_{\rm def}(\tilde{\varepsilon}_0)$ and $U\to\tilde{M}_{\rm def}(\tilde{\varepsilon}_0)$.

APPENDIX B: COUPLING COEFFICIENTS

The coupling coefficients of the symmetrized states of the defect surrounding are defined by

$$\xi_0(\kappa)=\xi_{A_{1g}}(\mathbf{k})\,\frac{1}{\sqrt{N}}\begin{cases}\beta_{\mathbf{k}} & \text{for } l=1\\ \gamma_{\mathbf{k}} & \text{for } l=2,\end{cases}$$
$$\xi_i(\kappa)=\xi_{E_i}(\mathbf{k})\,\frac{1}{\sqrt{N}}\begin{cases}\beta_{\mathbf{k}} & \text{for } l=1\\ \gamma_{\mathbf{k}} & \text{for } l=2,\end{cases} \tag{B1}$$

$i=1,2$ with

$$\xi_{A_{1g}}=\frac{\sqrt{2}}{\sqrt{3}}(\cos\mathbf{k}_x+\cos\mathbf{k}_y+\cos\mathbf{k}_z),$$
$$\xi_{E_1}=\frac{1}{\sqrt{3}}(2\cos\mathbf{k}_z-\cos\mathbf{k}_x-\cos\mathbf{k}_z), \tag{B2}$$
$$\xi_{E_2}=\tfrac{1}{2}(\cos\mathbf{k}_x-\cos\mathbf{k}_y),$$

and

$$\gamma_{\mathbf{k}}=\left[\tfrac{1}{2}\left(1-\frac{\varepsilon_{\mathbf{k}}-\tilde{\varepsilon}_f}{W_{\mathbf{k}}}\right)\right]^{1/2},$$
$$\beta_{\mathbf{k}}=-\left[\tfrac{1}{2}\left(1+\frac{\varepsilon_{\mathbf{k}}-\tilde{\varepsilon}_f}{W_{\mathbf{k}}}\right)\right]^{1/2}\mathrm{sgn}(\tilde{V}). \tag{B3}$$

[1] C. Weber, E. Sigmund, and M. Wagner, Phys. Rev. Lett. **55**, 1645 (1985).
[2] O. Brandt, E. Sigmund, and M. Wagner, Phys. Rev. B **49**, 5508 (1994).
[3] G. Wiese, H. Schäffer, and B. Elschner, Europhys. Lett. **11**, 791 (1990).
[4] H. Sturm, B. Elschner, and K. H. Höck, Phys. Rev. Lett. **54**, 1291 (1985).
[5] G. Travaglini and P. Wachter, Phys. Rev. B **29**, 893 (1984).
[6] P. A. Alekseev, A. S. Ivanov, B. Dorner, H. Schober, K. A. Kikoin, A. S. Mishchenko, V. N. Lazukov, E. S. Konovalova, Y. B. Paderno, A. Y. Rumyantsev, and I. P. Sadikov, Europhys. Lett. **10**, 457 (1989).
[7] T. H. Geballe, A. Menth, E. Buehler, and G. W. Hull, J. Appl. Phys. **41**, 904 (1970).
[8] S. E. Barnes, J. Phys. F **6**, 1375 (1976).
[9] P. Coleman, Phys. Rev. B **29**, 3035 (1983).
[10] H. Mori, Prog. Theor. Phys. **33**, 423 (1965); **34**, 399 (1965).
[11] C. Bloch and C. De Dominicis, Nucl. Phys. **7**, 459 (1956); **10**, 509 (1959).